Journal of Physics D: Applied Physics

LETTER

Directly-coupled well-wire hybrid quantum confinement lasers with the enhanced high temperature performance

To cite this article: Hanxu Tai *et al* 2023 *J. Phys. D: Appl. Phys.* **56** 23LT01

Letters

IOP Publishing

Journal of Physics D: Applied Physics

J. Phys. D: Appl. Phys. **56** (2023) 23LT01 (6pp)

https://doi.org/10.1088/1361-6463/acc874

Letter

Directly-coupled well-wire hybrid quantum confinement lasers with the enhanced high temperature performance

Hanxu Tai[1], Yuhong Wang[1], Ruonan Duan[1], Ming Zheng[1], Wei Lu[1], Yue Shi[1], Jianwei Zhang[2], Xing Zhang[2], Yongqiang Ning[2] and Jian Wu[1,*]

[1] School of Physics, Beihang University, Beijing 102206, People's Republic of China
[2] State Key Laboratory of Luminescence and Application, Changchun Institute of Optics, Fine Mechanics and Physics, Chinese Academy of Sciences, Changchun 130033, People's Republic of China

E-mail: jwu2@buaa.edu.cn

Received 1 December 2022, revised 6 March 2023
Accepted for publication 29 March 2023
Published 6 April 2023

Abstract

It is well known that the laser diode performance will inevitably deteriorate when the device is heated. It has been a difficult issue to solve to date. In this letter, we are reporting a new solution to improve high-temperature performance of the laser diodes. The device uses a kind of directly-coupled well-wire hybrid quantum confinement (HQC) structure of the active medium based on the InGaAs–GaAs–GaAsP material system. This special HQC structure is constructed based on the strain-driven indium (In)-segregation effect and the growth orientation-dependent on-GaAs multi-atomic step effect. The measurement and analysis for the HQC laser sample show that the carrier leakage loss, the Auger recombination and gain-peak shifting due to heating are reduced in the HQC structure. It therefore increases the optical gain for lasing at high temperature. The power conversion efficiency is enhanced by $>57\%$ and the threshold carrier density drops by $>24\%$ at $T \geqslant 360$ K, in comparison to the traditional quantum-well laser performance. A higher characteristic temperature of 240 K is obtained as well. It implies the better thermal stability of the HQC laser structure. These achievements show a significant prospect for developing high thermo-optic performance of laser diodes.

Keywords: semiconductor lasers, quantum well, quantum wires, thermal properties

(Some figures may appear in colour only in the online journal)

1. Introduction

The quantum-confined semiconductor lasers, e.g. quantum-well and quantum-dot lasers have been widely applied for various fields, including optical fiber communication, optical interconnection, atomic clock and scientific research, etc [1–3], where the InGaAs-based laser diodes show the promising prospects in generating terahertz (THz) waves, pumping the erbium-doped fiber lasers and amplifiers as well as achieving high power of short-wavelength laser devices (450–550 nm) by combining the second-harmonic generation, etc [4–6]. This is because there are higher barriers in the InGaAs quantum-confined laser structure, which enable the device to produce higher output power in the wavelength range of 900–1100 nm. However, the thermal effect always accompanies all semiconductor lasers and becomes more severe for high power of lasers. It will lead to laser diode performance

* Author to whom any correspondence should be addressed.

to inevitably deteriorate. Therefore, the thermal problem has been a bottleneck of development and application of the semiconductor lasers for ages.

In order to overcome thermal effect of the semiconductor lasers, some methods were investigated and applied in the past. A common approach is the use of external heat management [7]. However, this approach is not very effective to reducing interior heating of the laser medium and increases complexity of the laser device. Other ways include the improvement of laser structures, such as the uses of asymmetric waveguide [8–10] and low-dimensional structures (quantum wires or dots) [11, 12] as well as the application of the gain off-setting technique for single-frequency lasers [13]. With the asymmetric waveguide or simple low-dimensional structures, the improvement effect on reducing thermal-carrier loss for recombination is very limited. This can be reflected by their not-high characteristic temperatures of 100–130 K, in comparison with the usual characteristic temperature of 80–150 K from an InGaAs single quantum well (SQW) [14–16]. Theoretically, the higher is the characteristic temperature, the better is the thermal stability of the device [17]. In addition, a disadvantage of the quantum wires or dots is the lower optical gain and output power [18]. Their characteristic temperatures rapidly degenerate above the room temperature due to thermal escaping of the carriers [19]. The gain off-setting technique is used only for overcoming the thermal gain-shifting-induced loss in the single-frequency lasers at some temperature and not suitable for other types of laser diodes.

For the above reasons, we propose a new quantum-confined structure of lasers to enhance high-temperature performance of the device, which is an InGaAs-based directly-coupled well-wire hybrid quantum confinement (HQC) laser device. With such a special quantum-confined structure, the thermo-optic characteristics of the laser device can be improved so that the gain attenuation due to heating is restricted in the laser medium. The HQC laser structure and its thermal performance are described as follows.

2. Structural characterization and gain measurement

The laser structure is illustrated in figure 1. The kernel composition is the InGaAs–GaAs–GaAsP material system, where InGaAs is the active material. The active layer is composed of a 10 nm-thick well and self-assembled on-well wires. The wire height is ∼2 nm in average. The 2 nm-thick GaAs strain-compensating buffers are used between the InGaAs active layer and the 8 nm-thick GaAsP barrier layers. The GaAs buffers and GaAsP barriers together make up the step barriers in the energy-band structure. AlGaAs is the waveguide layer.

In the $In_xGa_{1-x}As$ well and wires, the indium (In) contents vary along the growth direction from 0 to 0.15 and from 0.15 to 0.17, respectively, due to the In-segregation effect [20]. The on-well wires are formed in a self-assembling way by the control of material growth direction on a slightly-misoriented GaAs(001) substrate so that the two-dimensional nucleation mode is changed to the step-flow mode during the material growth [21]. This is called growth orientation-dependent on-GaAs multi-atomic step effect and also the mechanism of the on-well wire formation [22]. In addition, as the strain in the well is partially released due to the In-segregation effect, the strain-caused morphological fluctuation of the well surface can be ignored. As the combination of wires and the well can enhance quantum confinement of the whole active structure, the thermo-optic performance of the device will be improved, comparing with a traditional quantum-confined laser diode.

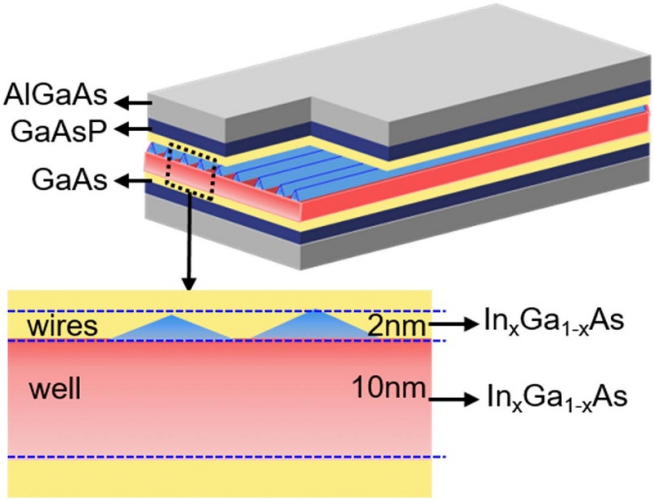

Figure 1. The illustration of the InGaAs HQC structure. The active layer contains a 10 nm thick well and the on-well wires with an average height of ∼2 nm.

The laser sample was grown on the GaAs (001) substrate in a slightly-misoriented direction under 100 mbar pressure and at a flow rate of 13 slm using the metal organic chemical vaporing deposition. The growth rate of the material was ∼1.0 μm h^{-1} at a V/III ratio of 50. A higher temperature of 650 °C was used for the InGaAs material growth to increase the migration distance of the In-atoms in the InGaAs active medium in light of the In-segregation effect. The on-well wires in the laser structure were morphologically observed and measured using an atomic force microscope (AFM, XE100) and a scanning electron microscope (SEM, Zeiss gemini300). A special sample with the exposed InGaAs surface was used for this purpose, which was fabricated under the same conditions by terminating its epitaxial growth just after completing the InGaAs layer formation. The results are shown in figures 2(a) and (b).

The length and height of the on-well wires are about 0.5–1.2 μm and 1.0–4.5 nm, respectively, according to the AFM and SEM measurement results, where the statistical analysis on the wire sizes shows that most of the wires are ∼2 nm in height and ∼90 nm in width. Thus, an averaged wire height of ∼2 nm is used in the subsequent analysis. In addition, the AFM tip-convolution effect on the wire height is ignored here, as it exists for both top and bottom measurements of the wires so that this error can be offset and thus should be negligible.

Figure 2(c) shows a cross-sectional image of the InGaAs active layer, which is obtained through the cross-sectional transmission electron microscope (X-TEM, JEM-2100F)

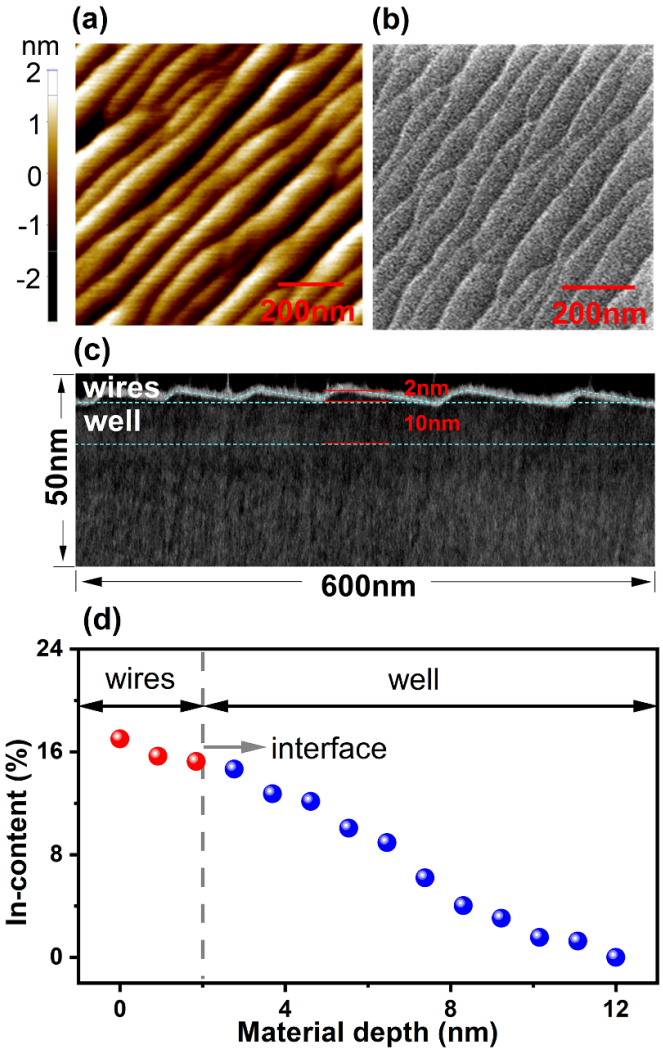

Figure 2. (a) and (b) The photographs of the on-well wires observed and measured using AFM and SEM, respectively. (c) The cross-sectional image of the InGaAs well and wires measured by X-TEM. (d) The In-content variation in the InGaAs layer in the material growth direction.

measurement. The image clearly shows the quantum wires formed on the well, in which the white outline is the focused ion beam influence on the InGaAs material in sample thinning processing. The width and height of the wires shown in the X-TEM image are consistent with the results from the AFM and SEM measurements. The In-content varying along the material growth direction in the InGaAs layer is measured using the x-ray photoelectron spectroscope (PHI Quantera II). The result is shown in figure 2(d). The above measurement results tell that the well width and the wire height are ∼10 nm and ∼2 nm, respectively and the In-content is monotonically changed approximately from 0 to 0.15 in the well and from 0.15 to 0.17 in the wires along the material growth direction.

In order to look at thermo-optic performance of the HQC laser structure, the thermal gain characteristics of the structure are measured at different temperatures. The measurement principle is briefly illustrated in figure 3. The sample for the gain measurement is a HQC edge-emitter with

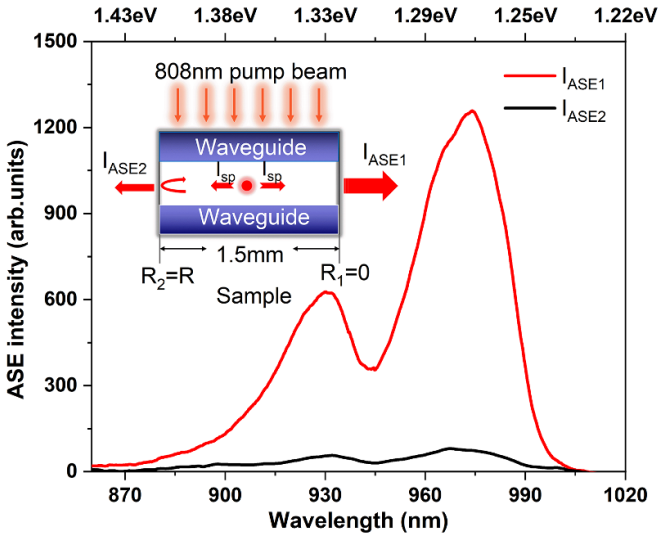

Figure 3. The TE-polarized ASE measurement from two facets of a HQC edge-emitter sample. The inset shows the principle of the ASE measurement. The optical injection power is 13.8 W.

1.5 mm × 0.5 mm in area, which is coated by the transmittance of $T = 99.99\%$ ($R_1 \approx 0$) at one facet and uncoated at the other facet ($R_2 = R \sim 0.3$ is determined by the InGaAs material index). The sample is optically pumped from the top using a beam of pulsed 808 nm laser with the pulse width of 20 ms.

Firstly, the amplified spontaneous emission (ASE) spectra of the HQC laser structure are measured from both ends of the edge-emitter and the results are shown in figure 3. We can clearly see from figure 3 that double peaks are formed in all spectra, in which the shorter wavelength peak at ∼930 nm is corresponding to the wire bandgap and the longer wavelength peak at ∼980 nm is corresponding to the well bandgap. Then, the modal gain G of the laser structure can be calculated by substituting the ASE data (I_{ASE1} and I_{ASE2}) into the following equation [23]:

$$G = \frac{1}{L}\ln\frac{(1-R)I_{\mathrm{ASE1}} - I_{\mathrm{ASE2}}}{RI_{\mathrm{ASE2}}} \tag{1}$$

where I_{ASE1} denotes the ASE intensity measured at the coated end of the sample, which is the sum of a single-pass ASE intensity and a round-trip ASE intensity from the same spontaneous emission (I_{sp}) source within the active layer. I_{ASE2} denotes only the single-pass ASE intensity measured at the uncoated end of the sample. L is the single-pass distance of light propagating through the device, which is $L = 1.5$ mm here.

3. Results and discussion

The temperature-dependent transverse electric (TE) polarized optical gains of the HQC laser structure are measured and shown in figure 4(a), where the injection power is 13.8 W and the device temperature is changed from 280 K to 360 K. The measured modal gain is converted into the material gain in figure 4(a) based on the relation of $g = (G + \langle\alpha_{\mathrm{i}}\rangle)/\Gamma$,

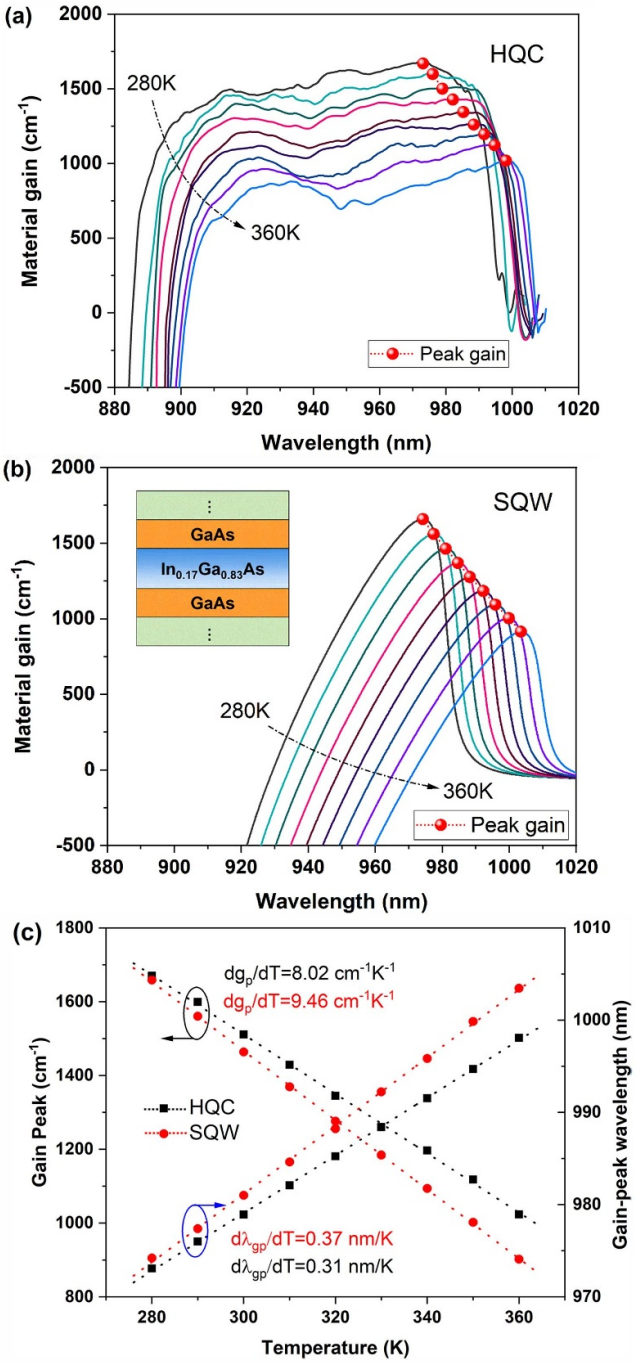

Figure 4. (a) The measured gain spectra of the InGaAs HQC structure in TE polarization mode at $T = 280$–360 K, where the modal gains are converted into the material gains here. The optical injection power is 13.8 W. (b) The calculated material gains of an InGaAs SQW with the same composition and size as the HQC structure under the same injection and temperature conditions. (c) Gain-peak variations with temperatures and thermal gain-peak shift in the two structures.

where Γ is the optical confinement factor of the laser structure, which equals to 0.02 for the given edge-emitter sample. $\langle\alpha_i\rangle \sim -6$ cm^{-1} is the averaged absorption loss coefficient of the InGaAs material, which is obtained from the measured modal gain. There are not apparent double peaks observed in the gain spectra in figure 4(a) because the gain spectra are broadened and become more uniform due to intermixing or superposing of wire and well gains. The In-content change in the InGaAs active layer is also a factor to form a more uniform gain spectrum.

For a comparison, we calculated the TE-polarized gain spectra as a function of temperature for an $In_{0.17}Ga_{0.83}As$ SQW model using the professional Photonic Integrated Circuit Simulator (PICS3D), as well. The calculation was completed based on the same structural composition, sizes and injection conditions. The results are shown in figure 4(b). We used a theoretical SQW model instead of a real device to compare the device performances here because it can conveniently achieve characteristic analysis of the devices under the completely identical conditions and avoid unnecessary errors and cost from the sample growth and fabrication. It is usually difficult to obtain different structures of samples with the completely identical growth and fabrication conditions in experiment.

In figures 4(a) and (b) the red spots are the gain peaks. By comparing the results in figures 4(a) and (b), we can observe two apparent differences of the thermal gain-peak variations from HQC and SQW structures, as is shown in figure 4(c). One is the thermal gain-peak attenuation reduced in the HQC structure, compared with the gain-peak variation in the SQW structure. Figure 4(c) gives the attenuation rates of thermal gain-peaks, dg_p/dT of the two structures, which are -8.02 cm^{-1} K^{-1} and -9.46 cm^{-1} K^{-1} for HQC and SQW structures, respectively. The difference of the gain-peak attenuations between the two structures is enlarged with increasing temperatures, which reaches $\sim$13.5% when the device is heated up to $T = 360$ K. It means that the gain loss of the InGaAs HQC structure is reduced by $\sim$13.5% at $T = 360$ K. The other is that the two structures show different thermal red-shift rates of the gain-peaks ($d\lambda_{gp}/dT$), which are 0.31 nm K^{-1} and 0.37 nm K^{-1} for HQC and SQW structures, respectively. The smaller thermal red-shift rate of the gain-peak together with the flatter gain spectrum shown in figure 4(a) from the HQC structure is specially meaningful to improving the single-frequency laser performance, as there is an additional gain loss that is induced by thermal gain red-shift effect in this sort of lasers. Thus, the less gain red-shift due to heating also reflects a better thermal stability of the HQC laser structure.

The causes why the directly-coupled well-wire HQC laser structure can demonstrate better thermal gain properties are associated with the quantum-wire modulation on the well and the reduced non-radiative recombination. On the one hand, the quantum wires enhance quantum confinement of the whole structure, resulting in the reduced carrier mobility and thus the reduction of carrier leakage loss at high temperature, compared with the SQW structure. On the other hand, there is a bigger transition distance (1.33 eV) between the first conduction sub-band (C_1) and the first valence sub-band of heavy holes (HH_1) in the quantum wires than in the well (1.26 eV), as illustrated in figure 5. Therefore, the Auger recombination coefficient of the whole structure can be reduced. The relevant studies on the non-radiative recombination have demonstrated that a larger bandgap of the material can result in a smaller Auger recombination coefficient [24], while a smaller

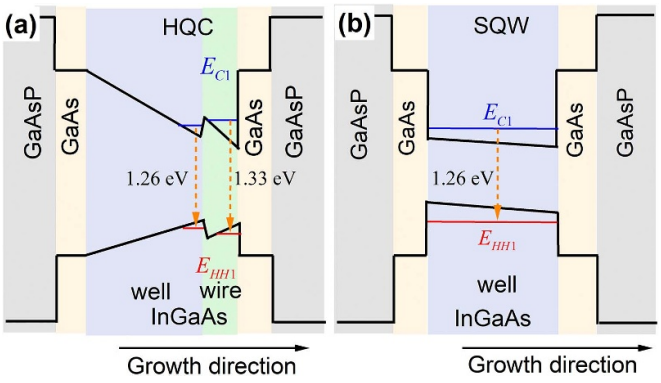

Figure 5. The diagrams of energy bands of (a) the InGaAs HQC structure and (b) the InGaAs SQW structure.

Auger recombination coefficient reflects the less non-radiative recombination. Thus, the HQC structure has a stronger ability against the thermal carrier loss associated with the non-radiative recombination, i.e. the better high-temperature performance. The bandgap difference between the InGaAs HQC and SQW structures is illustrated in figure 5, in which the inclined band-edges in figure 5(a) are formed from both compressive strains and continuous In-content changes in the well and wires, while the band-edge tilt in figure 5(b) is only due to the compressive strain in the well. There is a small band-edge step at the well-wire interface in figure 5(a), which is formed from the In-segregation-induced indium atom re-distribution on the well surface.

The threshold carrier density and the power conversion efficiency of the InGaAs HQC and SQW laser structures under various temperatures are calculated. The results are shown in figure 6(a), in which the black curves are the behavior of the HQC laser structure and the red curves are the behavior of a SQW structure. These calculations were completed under the same device dimensions to ensure the comparability of the results. The threshold carrier densities can be obtained by comparing the peak gains under different injection levels with the threshold gain. When the peak gain matches exactly the threshold gain, i.e. $g_{\text{peak}} = g_{\text{th}}$ at some injection level, the threshold carrier density can be determined. In this way, the threshold carrier density, J_{th} as a function of temperature can be obtained by repeating the above procedures at different temperatures. The threshold gain is obtained with the equation below,

$$g_{\text{th}} = \frac{\langle \alpha_{\text{i}} \rangle + \frac{1}{2L} \ln\left(\frac{1}{R_1 R_2}\right)}{\Gamma} \tag{2}$$

where R_1 and R_2 are the reflectivity of the laser cavity, which are $R_1 = R_2 \sim 0.3$ for the given edge-emitting laser sample here. Since both ends of the sample are uncoated, R_1 and R_2 are determined by the InGaAs material index. The cavity length is $L = 1.5$ mm. $\langle \alpha_{\text{i}} \rangle$ is ~ -6 cm^{-1}, which is obtained from the measured modal gain at room temperature (the modal gain has been converted as the material gain in figure 4(a)) and $\Gamma = 0.02$ for the given sample. The optical injection power is converted into the carrier density, J, according to the conversion relation with carrier density [25].

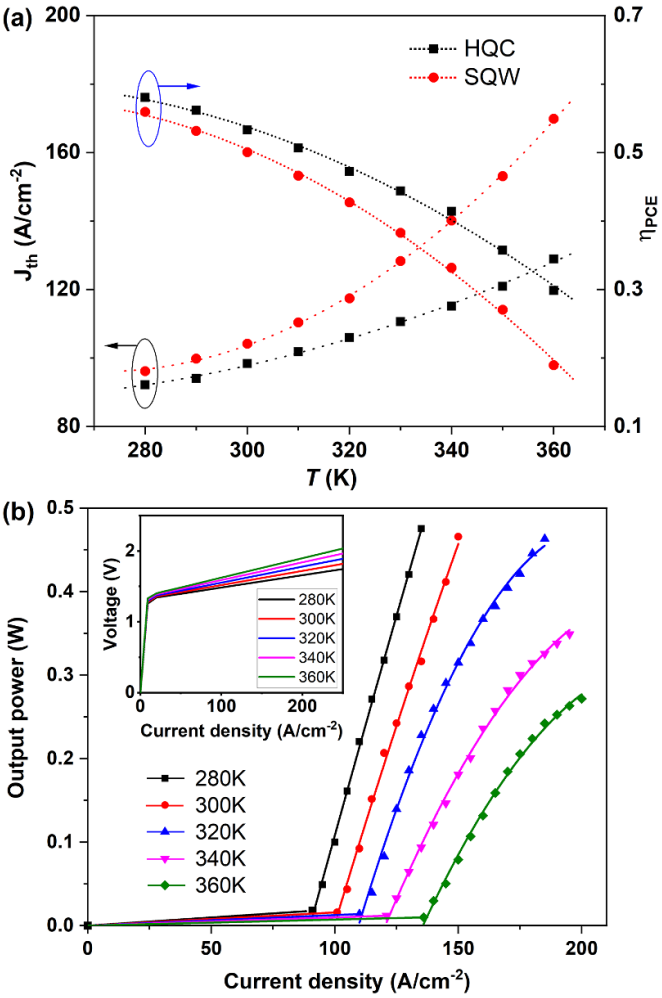

Figure 6. (a) Threshold current densities and power conversion efficiencies of the HQC and SQW laser structures as the functions of temperature. (b) Input–output characteristics of the InGaAs HQC laser sample.

The power conversion efficiency is calculated based on the definition below,

$$\eta_{\text{PCE}}(T) = \frac{P_{\text{out}}(T)}{P_{\text{pump}}(T)} \propto \frac{J(T) - J_{\text{th}}(T)}{J(T)} \tag{3}$$

where P_{pump} is the injection power, P_{out} is the output power and $P_{\text{out}} \propto (J - J_{\text{th}})$ [26].

The results in figure 6(a) show that the threshold carrier density, J_{th} is 24% lower from the HQC laser structure than from the SQW when the device temperature goes up to $T = 360$ K. Meanwhile, the power conversion efficiency of the HQC laser structure is correspondingly increased by 57% at $T = 360$ K, in comparison to the SQW laser structure performance. It can be predicted that the differences of threshold carrier densities and conversion efficiencies between the two laser structures will become bigger if the device is heated to higher temperatures than 360 K, according to the trends of threshold carrier density and power conversion efficiency developing with temperatures in figure 6(a). In addition, the characteristic temperature, T_0 of the device is calculated with the equation below [27]

$$\frac{1}{T_0} = \frac{1}{J_{\rm th}} \frac{{\rm d}J_{\rm th}}{{\rm d}T}. \quad (4)$$

For the HQC and SQW laser structures with the same device dimensions, their characteristic temperatures (T_0) are 240 K and 140 K, respectively, in the temperature range of 280–360 K. This result indicates that the HQC structure has the better thermal stability.

The input–output characteristics of the electrically-injected HQC laser sample are measured under different temperatures. The result is shown in figure 6(b), in which the inset is the *I*–*V* curves of the device. The result in figure 6(b) shows that the HQC laser device still works well without the use of any heat-sink means even if the device temperature is up to $T = 360$ K. This also confirms the validity of the InGaAs well-wire HQC laser structure in reducing the thermal carrier loss and enhancing the high-temperature performance of the laser diodes.

4. Conclusion

In this paper, a new laser structure with the enhanced high-temperature performance is reported here. The device uses the InGaAs directly-coupled well-wire HQC structure as the laser medium. The gain measurement and analysis for the HQC laser samples show that the proposed structure can reduce not only thermal carrier loss, but also thermal-shift of the gain-peak at higher temperatures, in comparison to the thermal performance of the traditional SQW laser diode. Subsequently, the characteristic temperature, the threshold carrier density, the power conversion efficiency and the input–output characteristics of the HQC laser device are calculated and measured as well. These results demonstrate the better high-temperature performance and thermal stability of the HQC laser structure than the traditional SQW laser device. The mechanism of the HQC laser structure enhancing thermal performance is analyzed with its special energy-band structure, which is associated with the strengthened carrier confinement and the reduced non-radiative recombination from the directly-coupled on-well quantum wires.

Data availability statement

All data that support the findings of this study are included within the article (and any supplementary files).

Acknowledgments

The authors gratefully acknowledge financial support from the National Natural Science Foundation of China (Grant No. 61874117) for this work.

ORCID iD

Jian Wu https://orcid.org/0000-0003-1434-7673

References

[1] Liu A, Wolf P, Lott J A and Bimberg D 2019 *Photon. Res.* **7** 121–36
[2] Souto J, Luis Pura J and Jimenez J 2019 *J. Phys. D: Appl. Phys.* **52** 343002
[3] Zhang J, Ning Y, Zeng Y, Zhang J, Zhang J, Fu X, Tong C and Wang L 2013 *Laser Phys. Lett.* **10** 045802
[4] Hoffmann S and Hofmann M R 2007 *Laser Photonics Rev.* **1** 44–56
[5] Yang G W, Smith G M, Davis M K, Loeber D A S, Hu M, Zah C E and Bhat R 2004 *IEEE Photonics Technol. Lett.* **16** 2403–5
[6] Kim J-Y, Cho S, Lim S-J, Yoo J, Kim G B, Kim K-S, Lee J, Lee S-M, Kim T and Park Y 2007 *J. Appl. Phys.* **101** 033103
[7] Zolotovskaya S A, Daghestani N, Venus G B, Glebov L B, Smirnov V I and Rafailov E U 2007 *Appl. Phys. Lett.* **91** 171113
[8] Ryvkin B and Avrutin E 2009 *J. Appl. Phys.* **105** 103107
[9] Li L, Liu G, Li Z, Li M, Li H, Wang X and Wan C 2008 *IEEE Photonics Technol. Lett.* **20** 566–8
[10] Wang H, Yu H, Zhou X, Kan Q, Yuan L, Chen W, Wang W, Ding Y and Pan J 2014 *Appl. Phys. Lett.* **105** 141101
[11] Klopf F, Reithmaier J P and Forchel A 2000 *Appl. Phys. Lett.* **77** 1419–21
[12] Arsenijevic D, Liu C, Payusov A, Stubenrauch M and Bimberg D 2012 *IEEE Photonics Technol. Lett.* **24** 906–8
[13] Li H, Wolf P, Jia X, Lott J A and Bimberg D 2017 *Appl. Phys. Lett.* **111** 243508
[14] Wiedmann N, Jandeleit J, Mikulla M, Kiefer R, Bihlmann G, Poprawe R and Weimann G 2001 *Proc. SPIE* **4283** 247–55
[15] Miah M J, Kettler T, Posilovic K, Kalosha V P, Skoczowsky D, Rosales R, Bimberg D, Pohl J and Weyers M 2014 *Appl. Phys. Lett.* **105** 151105
[16] Duffy D A, Marko I P, Fuchs C, Eales T D, Lehr J, Stolz W and Sweeney S J 2021 *J. Phys. D: Appl. Phys.* **54** 365104
[17] Jiang L and Asryan L V 2007 *Laser Phys. Lett.* **4** 265–9
[18] Maximov M V *et al* 2020 *Appl. Sci.* **10** 1038
[19] Amanai H, Nagao S and Sakaki H 2003 *J. Cryst. Growth* **251** 223–9
[20] Yu H, Roberts C and Murray R 1995 *Appl. Phys. Lett.* **66** 2253–5
[21] Dong H, Sun J, Ma S, Liang J, Lu T, Liu X and Xu B 2016 *Nanoscale* **8** 6043–56
[22] Lee S, Akabori M and Shirahata T 2001 *J. Cryst. Growth* **231** 75–81
[23] Ma M L, Wu J, Ning Y Q, Zhou F, Yang M, Zhang X, Zhang J and Shang G Y 2013 *Opt. Express* **21** 10335–41
[24] Masse N F, Adams A R and Sweeney S J 2007 *Appl. Phys. Lett.* **90** 161113
[25] Kuznetsov M, Hakimi F, Sprague R and Mooradian A 1999 *IEEE J. Sel. Top. Quantum Electron.* **5** 561–73
[26] Yang G W, Hwu R J, Xu Z T and Ma X Y 2000 *IEEE J. Sel. Top. Quantum Electron.* **6** 577–84
[27] Korpijarvi V-M, Viheriala J, Koskinen M, Aho A T and Guina M 2016 *Opt. Lett.* **41** 657–60